NEUROSCIENCE

Molecular beacon–based detection of circulating microRNA-containing extracellular vesicle as an α-synucleinopathy biomarker

Zhenwei Yu[1,2]†, Yuanchu Zheng[2,3]†, Huihui Cai[2,3], Siming Li[2,3], Genliang Liu[2,3], Wenyi Kou[2,3], Chen Yang[2,3], Shuangshuang Cao[4], Lei Chen[5], Xuedong Liu[6], Zhirong Wan[7], Ning Zhang[8], Xiaohong Li[9], Guiyun Cui[10], Ying Chang[11], Yue Huang[2,12,13], Hong Lv[14], Tao Feng[2,3]*

Early and precise diagnosis of α-synucleinopathies is challenging but critical. In this study, we developed a molecular beacon–based assay to evaluate microRNA-containing extracellular vesicles (EVs) in plasma. We recruited 1203 participants including healthy controls (HCs) and patients with isolated REM sleep behavior disorder (iRBD), α-synucleinopathies, or non–α-synucleinopathies from eight centers across China. Plasma miR-44438–containing EV levels were significantly increased in α-synucleinopathies, including those in the prodromal stage (e.g., iRBD), compared to both non–α-synucleinopathy patients and HCs. However, there are no significant differences between Parkinson's disease (PD) and multiple system atrophy. The miR-44438–containing EV levels negatively correlated with age and the Hoehn and Yahr stage of PD patients, suggesting a potential association with disease progression. Furthermore, a longitudinal analysis over 16.3 months demonstrated a significant decline in miR-44438–containing EV levels in patients with PD. These results highlight the potential of plasma miR-44438–containing EV as a biomarker for early detection and progress monitoring of α-synucleinopathies.

INTRODUCTION

Parkinson's disease (PD), as well as other α-synucleinopathies such as multiple system atrophy (MSA), is characterized by α-synuclein (α-syn) accumulation in both the brain and the peripheral nervous system (*1*). The precise and early diagnosis of these diseases can be difficult, considering the complexity and heterogeneity of the symptoms (*2*, *3*). There is an urgent need for an easy and reliable assay that can diagnose α-synucleinopathies precisely and early (*4*).

MicroRNAs (miRNAs) are small noncoding RNAs that regulate gene expression and modify metabolic pathways. They can act as modulators and biomarkers for various diseases, including α-synucleinopathies, which are caused by the abnormal accumulation of α-syn in the brain (*5*). Several studies and reviews have explored the role of miRNAs in the diagnosis and pathological pathways of α-synucleinopathies (*6*, *7*). We recently reported that the concentration of miR-44438, a recently found miRNA, is increased in the neuron-derived extracellular vesicles (EVs) from the plasma of patients with PD compared to those from healthy controls (HCs). Furthermore, this miRNA is implicated in the exosome generation and α-syn secretion in dopaminergic neurons (*8*).

The blood-brain barrier serves as a protective shield against peripheral macromolecules, yet it poses challenges in monitoring the brain via peripheral biofluids. Recent insights suggested that certain pathological molecules, like amyloid-β, tau, and α-syn, may traverse the blood-brain barrier when encapsulated within EVs (*9*). We have also shown that oligodendrocyte-derived (CNPase-positive) EVs can be detected in peripheral blood using fluorescence nanoparticle tracking analysis (NTA) (*10*). However, this approach requires highly stable fluorescent conjugates, such as quantum dots, to label the target protein on EVs, limiting its utility. A recent technology that has emerged is nanoscale flow cytometry, which can identify and quantify EVs carrying specific proteins in cerebrospinal fluid and blood. This technology allows the classification of EVs derived from different cell types; for instance, NCAM, L1CAM, and NMDAR2A distinguish neuron-derived EVs (*11*), and CD62P is indicative of EVs likely originating from platelets (*12*). While numerous miRNAs have been implicated in the pathogenesis of neurodegenerative diseases like PD (*5*, *13*, *14*), the characterization of miRNA-containing EVs remains unexplored.

Molecular beacons (MBs) are oligonucleotide probes that have a stem-loop hairpin structure and emit fluorescence when they hybridize with target DNA or RNA sequences (*15*). However, these probes suffer from cross-quenching when they detect miRNAs in a confined space, such as exosomes, which suppresses the fluorescent signal and detection sensitivity. Mao *et al.* (*16*) recently developed a nano-cage MB (NCMB) that encloses the quencher and the fluorophore in a DNA cube. When the target miRNA binds to the NCMB, the fluorophore is released from the cube, while the quencher remains inside. This assay minimizes the cross-quenching effect and enables the in situ analysis of target miRNAs in biofluids and exosomes.

[1]Department of Pathophysiology, Beijing Neurosurgical Institute, Capital Medical University, Beijing, China. [2]Center for Movement Disorders, Department of Neurology, Beijing Tiantan Hospital, Capital Medical University, Beijing, China. [3]China National Clinical Research Center for Neurological Diseases, Beijing Tiantan Hospital, Capital Medical University, Beijing, China. [4]Department of Neurology, Yidu Central Hospital of Weifang, Shandong, China. [5]Department of Neurology, Tianjin Huanhu Hospital, Tianjin, China. [6]Department of Neurology, Fourth Military Medical University, Xi'an, China. [7]Department of Neurology, Aerospace Center Hospital, Beijing, China. [8]Department of Neuropsychiatry and Behavioral Neurology and Clinical Psychology, Beijing Tiantan Hospital, Capital Medical University, Beijing, China. [9]Department of Neurology, Dalian Friendship Hospital, Dalian, China. [10]Department of Neurology, Affiliated Hospital of Xuzhou Medical University, Xuzhou, China. [11]Department of Neurology, China-Japan Union Hospital of Jilin University, Changchun, China. [12]Human Brain and Tissue Bank, China National Clinical Research Center for Neurological Diseases, Beijing Tiantan Hospital, Capital Medical University, Beijing, China. [13]Department of Pharmacology, School of Biomedical Sciences, Faculty of Medicine and Health, UNSW Sydney, Sydney, NSW, Australia. [14]Department of Clinical Diagnosis, Beijing Tiantan Hospital, Capital Medical University, Beijing, China.
*Corresponding author. Email: bxbkyjs@sina.com
†These authors contributed equally to this work.

In the current study, we modified the NCMB probe and made it suitable for detecting and quantifying plasma miR-44438–containing EV levels using nanoscale flow cytometry assay. We measured the plasma miR-44438–containing EV concentrations in a training cohort to distinguish PD, MSA, progressive supranuclear palsy (PSP), and HCs. We confirmed the difference between PD and HCs in a multicenter validation cohort. We also analyzed the correlations of miR-44438–containing EV levels with demographic and clinical characteristics. Next, we followed a PD longitudinal cohort to monitor the changes in plasma miR-44438–containing EV concentrations with disease progression. Last, we evaluated the plasma miR-44438–containing EV levels in an isolated rapid eye movement (REM) sleep behavior disorder (iRBD) cohort to test the potential of this biomarker for the early diagnosis of α-synucleinopathies at the prodromal stage.

RESULTS

Participant characteristics

A total of 1203 participants were included in this study. For the discovery cohort, 718 participants including 302 patients with PD [median (range) age, 66 (36 to 85) years; 135 female (44.7%); 167 male (55.3%)], 119 patients with MSA [median (range) age, 62 (41 to 80) years; 60 female (50.4%); 59 male (49.6%)], 21 patients with PSP [median (range) age, 65 (56 to 77) years; 10 female (47.6%); 11 male (52.4%)], and 276 HCs [median (range) age, 60 (49 to 76) years; 126 female (45.7%); 150 male (54.3%)] were recruited from Beijing Tiantan Hospital. For the validation cohort, we recruited 208 patients with PD [median (range) age, 66 (34 to 87) years; 98 female (47.1%); 110 male (52.9%)] and 217 HCs [median (range) age, 60 (51 to 89) years; 96 female (44.2%); 121 male (55.7%)] from eight PD centers in China. Furthermore, we recruited a longitudinal cohort containing 88 patients with PD [38 female (43.2%); 50 male (56.8%); median (range) age, 66.5 (33 to 86) years at baseline visit and 68 (36 to 87) at the follow-up visit]. We also recruited a cohort containing 30 patients with iRBD [median (range) age, 65 (43 to 78) years; 8 female (26.7%); 22 male (73.3%)] and 30 HCs [median (range) age, 59 (55 to 71) years; 13 female (43.3%); 17 male (56.7%)] to investigate the miR-44438–containing EV levels in the prodromal condition of α-synucleinopathies. The race of all participants was Asian. Demographic and clinical characteristics of all participants were reported in Table 1.

The construction and characterization of NCMB

The schematic illustration for the NCMB construction is presented in Fig. 1A. Briefly, the DNA strands (NCMB1, NCMB2, NCMB3, NCMB4, NCMB-assist, NCMB-anchor, and NCMB-BHQ2; table S1) were mixed to generate a DNA scaffold by cross-hybridization. Then, the NCMB-cy3 strand was added to the DNA scaffold for the construction of active NCMB. We also visualized the NCMB by using transmission electron microscopy (TEM) (Fig. 1B). The workflow for the sample preparation and the nanoscale flow cytometry assay is presented in Fig. 1C. The NCMB was further tested for the detection of target miRNA. The miR-44438 mimic with different concentrations was added to the miR-44438–NCMB solution, and the fluorescent intensity was measured. We found that the cy3 fluorescent intensity of miR-44438–NCMB significantly increased with the presence of miR-44438 mimic, but the fluorescent intensity remained at a low level when three irrelevant miRNA (miR22, miR151, and miR191) mimics were added as negative controls (Fig. 1D). The fluorescent intensity was positively correlated with the miR-44438 mimic concentrations (Fig. 1E). Next, we tested the detection of target miRNA–containing EVs in plasma using the NCMB. The Apogee Mix containing a set of fluorescent beads of known size (110 and 500 nm) was run at the beginning of every daily calibration to test the performance of the CytoFLEX S flow cytometer (Fig. 1F). A reference plasma with different dilutions was mixed and incubated with miR-44438–NCMB, and the total gated events were calculated to test the reliability of this assay (Fig. 1G). Furthermore, we tested the reproducibility of this assay over three freeze and thaw cycles using two independent reference plasma samples (Fig. 1H). In addition, we labeled the miR-44438–containing EVs with other markers that were indicative of the sources of these EVs in five reference plasma samples. The results demonstrated that more than half of the miR-44438–containing EVs were derived from neurons (65.9% $L1CAM^+$; 49.3% $NMDAR2A^+$), and only 3.6% of miR-44438–containing EVs are CD62P positive (fig. S1).

Group comparisons of plasma miR-44438–containing EV concentrations

We compared the plasma miR-44438–positive EV concentrations in the discovery cohort including 302 patients with PD, 119 patients with MSA, 21 patients with PSP, and 276 HCs. The gating strategy for the detection of miR-44438–containing EVs was presented in Fig. 2A. The representative images of the nanoscale flow cytometry assay were shown in Fig. 2B. The plasma miR-44438–containing EV concentrations were significantly increased in patients with PD or MSA than those in patients with PSP or HCs, with the controlling of age, sex, and body mass index (BMI) (Fig. 2C). Notably, there were no significant differences between PD and MSA groups for plasma miR-44438–containing EV concentrations. The receiver operating characteristic (ROC) curve analysis confirmed that the plasma miR-44438–containing EV concentrations were highly accurate in discriminating PD from HCs [Fig. 2D; area under curve (AUC) = 0.947, 95% confidence interval (CI) 93.1 to 96.4%, sensitivity 88.4%, 95% CI 84.3 to 91.6%, specificity 86.6%, 95% CI 82.1 to 90.1%] and in discriminating MSA from HCs (Fig. 2D; AUC = 0.912, 95% CI 88.2 to 94.2%, sensitivity 84.0%, 95% CI 76.4 to 89.5%, specificity 85.9%, 95% CI 81.3 to 89.5%). The AUC for PSP versus HC was 0.816 (Fig. 2D; 95% CI 73.5 to 89.7%, sensitivity 81.0%, 95% CI 60.0 to 92.3%, specificity 74.3%, 95% CI 68.8 to 79.1%). The ROC curves for the differentiation of patients with PSP from patients with PD or MSA were presented in fig. S2 (AUC_{PD} versus $_{PSP}$ = 0.829, 95% CI 76.1 to 89.6%, sensitivity 95.24%, 95% CI 77.3 to 99.8%, specificity 61.26%, 95% CI 55.7 to 66.6%; AUC_{MSA} versus $_{PSP}$ = 0.754, 95% CI 66.2 to 84.5%, sensitivity 95.24%, 95% CI 77.3 to 99.8%, specificity 51.26%, 95% CI 42.4 to 60.1%).

The difference between patients with PD and HCs was replicated in a multi-center validation cohort including 208 patients with PD and 217 HCs. We also observed significantly higher plasma miR-44438–containing EV concentrations in patients with PD than those in HCs (Fig. 2E; $P < 0.001$), with an AUC of 0.909 (Fig. 2F; 95% CI 88.2 to 93.6%, sensitivity 76.4%, 95% CI 70.2 to 81.7%, specificity 91.7%, 95% CI 87.3 to 94.7%).

Furthermore, we visualized the miR-44438 level with miR-44438–NCMB probe in the midbrain slices from one pathology-confirmed PD patient and three non-PD controls. We also analyzed the α-syn levels by using immunofluorescence staining (fig. S3A). The results showed a significant increase of both α-syn (fig. S3B) and miR-44438

Table 1. Summary of the demographics and clinical data of participants. PD, patients with Parkinson's disease; HC, health controls; iRBD, isolated REM behavior disorder; UPDRS III, Movement Disorder Society–sponsored Unified Parkinson Disease Rating Scale Part III; H&Y, Hoehn and Yahr scale; MMSE, Mini-MentalState Examination; MoCA, Montreal Cognitive Assessment; RBDSQ, Rapid Eye Movement Sleep Behavior Disorder Questionnaire.

Discovery cohort	Diagnosis	PD	MSA	PSP	HC
	Number	302	119	21	276
	Age, median (range)	66 (36–85)	62 (41–80)	65 (56–77)	n(49–76)
	Sex (male: female)	167:135	59:60	11:10	150:126
	Disease duration, year, median (range)	7 (0.5–26)	2.5 (0.5–8)	3 (1.5–8)	NA
	UPDRS III, median (range)	40.5 (4–84)	42 (10–89)	38.5 (16–77)	NA
	H&Y, median (range)	3 (1–5)	NA	NA	NA
	MMSE, median (range)	27 (10–30)	27 (10–30)	22 (7–29)	NA
	MoCA, median (range)	22 (5–30)	21 (2–30)	16 (4–25)	NA
Validation cohort	Diagnosis	PD		HC	
	Number	208		217	
	Age, median (range)	66 (34–87)		60 (51–89)	
	Sex (male:female)	110:98		121:96	
	Disease duration, year, median (range)	6 (0.25–25)		NA	
	UPDRS III, median (range)	39 (8–110)		NA	
	H&Y, median (range)	3 (1–5)		NA	
	MMSE, median (range)	26 (6–30)		NA	
	MoCA, median (range)	21 (4–30)		NA	
Prodromal cohort	Diagnosis	iRBD		HC	
	Number	30		30	
	Age, median (range)	65 (43–78)		59 (55–71)	
	Sex (male:female)	22:8		17:13	
	Disease duration, year, median (range)	5 (0.5–40)		NA	
	UPDRS III, median (range)	4 (0–25)		NA	
	MMSE, median (range)	28 (21–30)		NA	
	MoCA, median (range)	23 (17–28)		NA	
	RBDSQ, median (range)	7 (3–10)		NA	
Longitudinal cohort	Diagnosis		PD		
		Baseline		Follow-up	
	Number		88		
	Age, median (range)	66.5 (33–86)		68 (36–87)	
	Sex (male:female)		55:33		
	Disease duration, year, median (range)	6 (0.5–19)		7 (1.5–21)	
	UPDRS III, median (range)	36.5 (5–76)		39 (7–84)	
	H&Y, median (range)	3 (0–5)		3 (1–5)	
	MMSE, median (range)	27 (17–30)		26 (10–30)	
	MoCA, median (range)	21 (8–30)		21 (5–29)	

(fig. S3C) levels in the midbrain of a patient with PD compared to those in HCs. In addition, we noticed a colocalization of α-syn and miR-44438 in PD patient's midbrain (fig. S3A, arrows).

We also assessed the size distributions (fig. S4, A to E) and concentrations (fig. S4F) of plasma EVs from HCs and patients with PD, MSA, PSP, or iRBD by using NTA. The results indicated no significant differences in either size distribution or concentration across these groups.

Correlations of plasma miR-44438–containing EV concentrations with demographic and clinical characteristics of patients with PD

Next, we analyzed the correlation of plasma miR-44438–containing EV concentrations with demographic and clinical characteristics including age, sex, disease duration, Mini-Mental State Examination (MMSE) score, Montreal Cognitive Assessment (MoCA) scale,

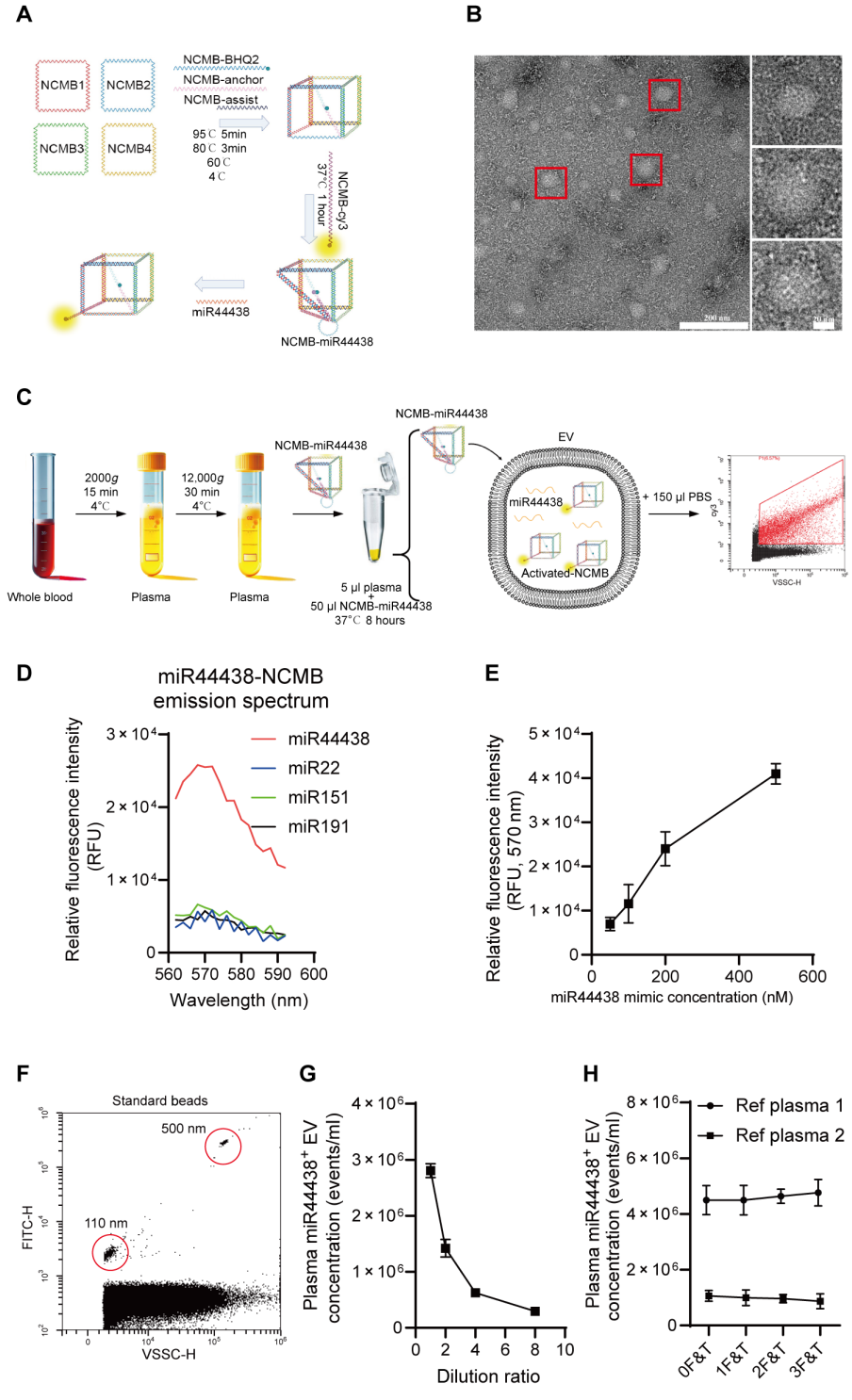

Fig. 1. Schematic illustration and characterization of NCMB. (**A**) Schematic illustration of miR- 44438–NCMB construction. (**B**) TEM images of NCMBs with the presence of miR-44438 mimics. (**C**) Illustration of the workflow to the nanoscale flow cytometry assay. (**D**) Fluorescence intensity of miR-44438–NCMB responding to miR-44438 mimic or irrelevant miRNA mimics. (**E**) Correlation between miR- 44438 mimic concentration and fluorescence intensity of NCMB at 570 nm. (**F**) Characterization of Apogee Mix standard beads using the nanoscale flow cytometry assay. (**G**) miR- 44438–NCMB responding to serial dilutions of reference plasma by using nanoscale flow cytometry assay. (**H**) Concentrations of miR-44438–positive EVs in two reference plasma samples subjected to zero to three freeze-thaw cycles.

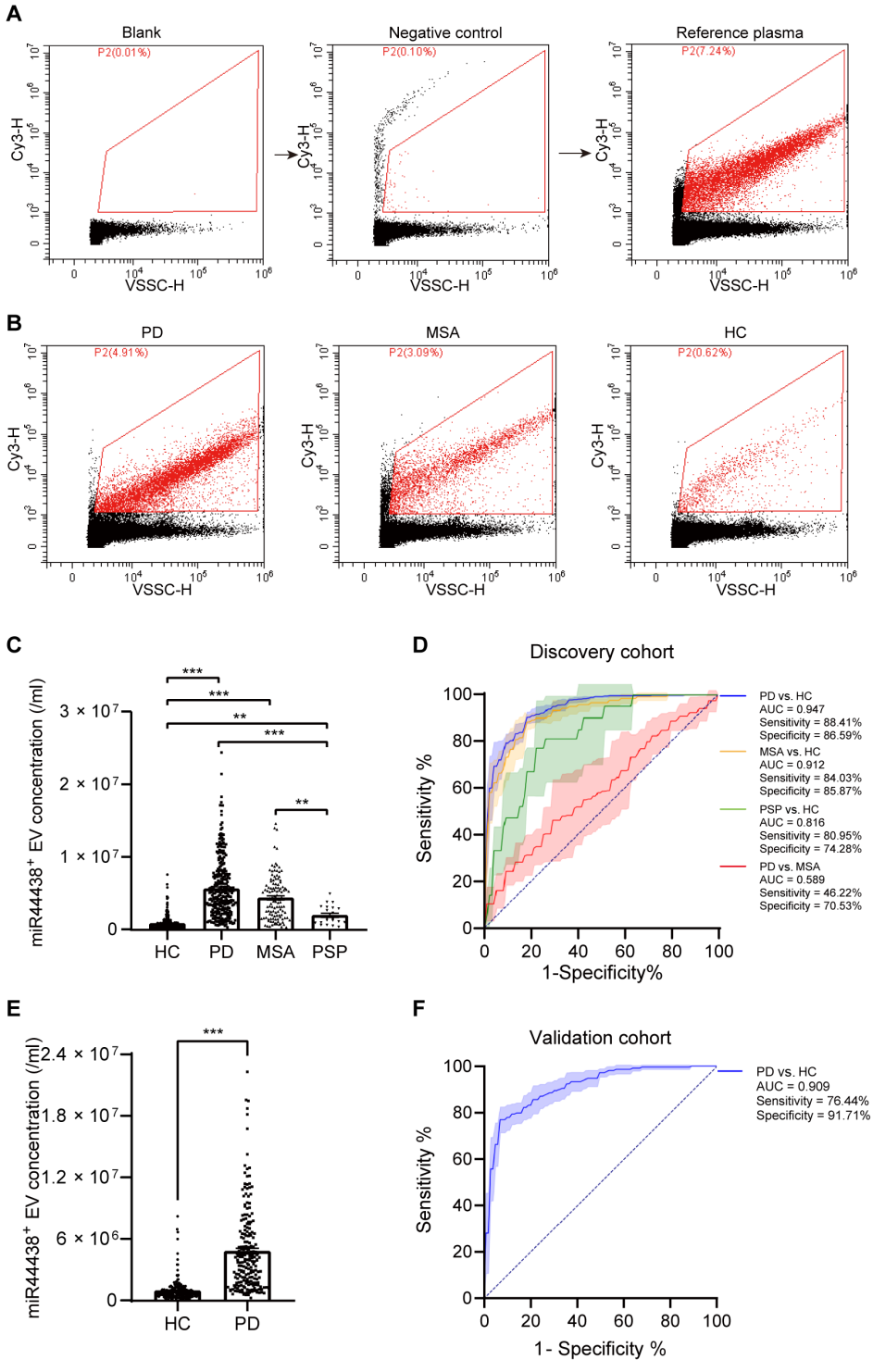

Fig. 2. Comparison of plasma miR-44438–containing EV levels between groups. (**A**) Gating strategy for the detection of miR-44438–containing EVs in plasma. (**B**) Representative images of nanoscale flow cytometry assay. (**C**) Plasma miR-44438–containing EV concentrations in patients with PD, MSA, and PSP and HCs in the discovery cohort. ***$P < 0.001$; **$P < 0.01$. (**D**) ROC curves of plasma miR-44438–containing EVs for discriminating patients with PD, MSA, and PSP and HCs in the discovery cohort. (**E**) Plasma miR-44438–containing EV concentrations in patients with PD and HCs in the validation cohort. ***$P < 0.001$. (**F**) ROC curve of plasma miR-44438–containing EVs for discriminating patients with PD from HCs in the validation cohort.

Hoehn-Yahr (H&Y) scale, Movement Disorder Society Unified Parkinson's Disease Rating Scale Part III (MDS-UPDRS III), Levodopa Equivalent Daily Dose (LEDD), and BMI in patients with PD ($n = 510$). We observed significantly negative correlations of plasma miR-44438–containing EV concentrations with age [Fig. 3, A and B; $R = -0.143$ (95% CI, −0.229 to −0.054); $P = 0.001$], H&Y scale [Fig. 3, A and C; $R = -0.130$ (95% CI, −0.218 to −0.040); $P = 0.004$], and BMI [Fig. 3A; $R = 0.134$ (95% CI, 0.033 to 0.233); $P = 0.008$] of patients with PD. A significant but weak correlation was observed for the plasma miR-44438–containing EV concentrations with the onset age [Fig. 3A; $R = -0.116$ (95% CI, −0.206 to −0.025); $P = 0.01$] of patients with PD. Results for the correlations of miR-44438–containing EV concentrations and other characteristics were presented in table S2.

Changes of plasma miR-44438–containing EV concentrations in a longitudinal PD cohort

To further investigate the correlation of miR-44438–containing EV levels and the disease progression, we next tested the change of miR-44438–containing EV levels in a longitudinal cohort including 88 patients with PD. We used a mixed-effect model with the controlling of age and found a significant decrease of plasma miR-44438–containing EV levels (Fig. 3D; $P < 0.001$) in patients with PD after a mean interval of 16.3 months. Furthermore, we assessed the differences in miR-44438–containing EV levels between HCs and patients with PD, both at baseline and during follow-up visits. Our findings indicated that although miR-44438–containing EV levels decrease as PD progresses, they remain significantly higher in patients with PD at follow-up visits compared to HCs.

Plasma miR-44438–containing EV concentrations in early-stage PD

Considering that the plasma miR-44438–containing EV levels of patients with PD decline as the disease progresses, this biomarker may drop to the HC range at the late-stage of PD in some patients. We used the Youden index to obtain a cutoff value that discriminates patients with PD from HCs using the combination of the discovery cohort and the validation cohort and compared the H&Y scale between the false-negative patients with PD and the rest. A significantly higher H&Y scale in patients with false-negative PD compared to those in the positive subgroup was observed (Fig. 4A; $P < 0.001$), which may weaken the efficacy of the plasma miR-44438–containing EV as a diagnostic biomarker of PD. We also compared the miR-44438–containing EVs in HCs and patients with PD at an early or late stage that were characterized by H&Y scale (Fig. 4B and

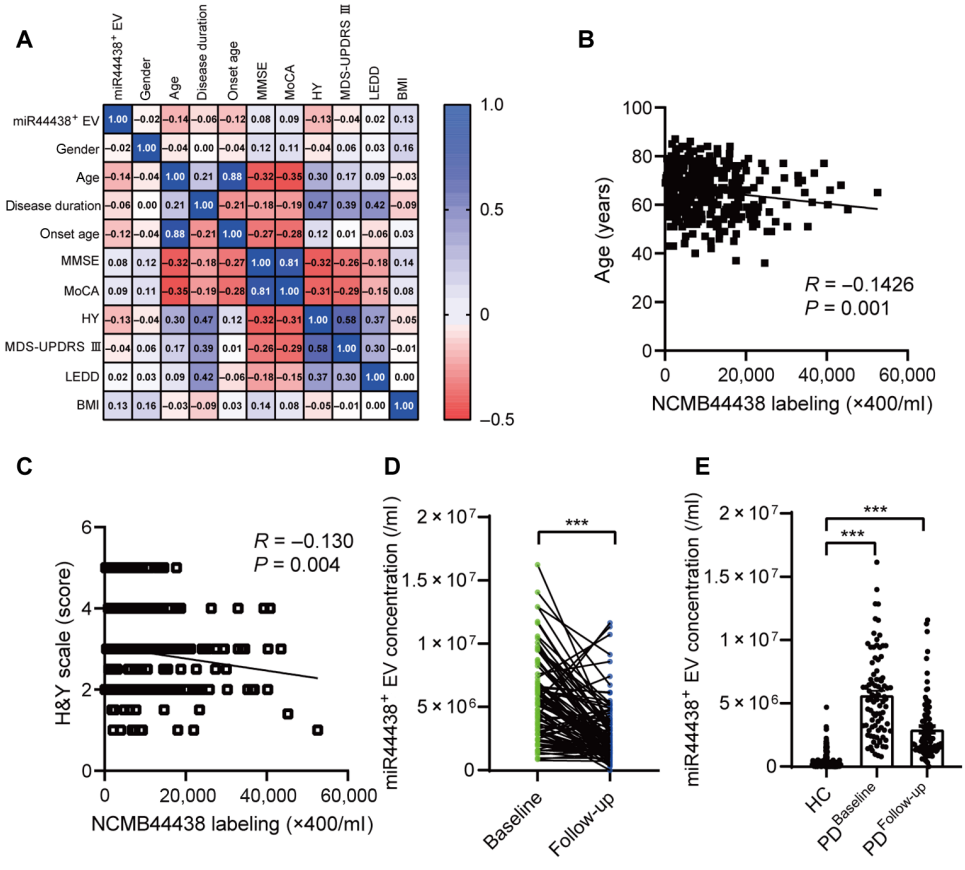

Fig. 3. Correlation analysis and a longitudinal study of miR-44438–containing EV levels in patients with PD. (**A**) Correlation analysis between plasma miR-44438–containing EV concentrations and sex, age, age at onset, MMSE, MoCA, H&Y stage and UPDRS III score, LEDD, and BMI of patients with PD. (**B**) Correlation analysis between plasma miR-44438–containing EV concentrations and age. (**C**) Correlation analysis between plasma miR-44438–containing EV concentrations and H&Y scales. (**D**) Plasma miR-44438–containing EV concentrations at baseline and follow-up visits in the longitudinal PD cohort. (**E**) Comparisons of plasma miR-44438–containing EV concentrations between HCs and patients with PD at both baseline visit and follow-up visit. ***$P < 0.001$.

table S3; H&Y < 2.5 versus H&Y = 4 to 5) or disease duration (Fig. 4D and table S3; disease duration ≤5 years versus disease duration >5 years). Notably, PD precise diagnosis is challenging mainly at the early stage rather than the late stage. We found that the efficacy of plasma miR-44438–containing EV levels in diagnosing patients with PD with H&Y ≤ 2.5 is performing better than those in discriminating all patients with PD from HCs, with the AUC increasing from 0.935 (Fig. 4C; 95% CI 91.8 to 95.2%, sensitivity 85.1%, 95% CI 81.8 to 87.9%, specificity 86.2%, 95% CI 81.7 to 89.8%, all PD versus HCs) to 0.951 (Fig. 4C; 95% CI 93.2 to 97.0%, sensitivity 90.5%, 95% CI 85.5 to 93.9%, specificity 86.6%, 95% CI 82.1 to 90.1%, $PD^{H\&Y \leq 2.5}$ versus HCs). Similarly, the AUC for discriminating patients with PD with disease duration ≤5 years from HCs is 0.945 (Fig. 4E; 95% CI 92.7 to 96.3%, sensitivity 87.6%, 95% CI 82.3 to 91.4%, specificity 88.8%, 95% CI 85.8 to 91.3%, $PD^{\text{Disease duration} \leq 5}$ versus HCs) and for discriminating patients with PD with disease duration >5 years from HCs is 0.922 (Fig. 4E; 95% CI 90.2 to 94.1%, sensitivity 82.0%, 95% CI 76.9 to 86.1%, specificity 86.8%, 95% CI 83.5 to 89.5%, $PD^{\text{Disease duration} > 5}$ versus HCs).

Validation of the miR-44438–containing EV levels in patients with iRBD

iRBD is generally considered a prodromal stage of α-synucleinopathies. We next tested the utility of plasma miR-44438–containing EV concentrations to differentiate patients with iRBD from HCs. The results showed that this biomarker is significantly higher in patients with iRBD than in HCs (Fig. 5A; $P < 0.01$). ROC analysis demonstrated an AUC of 0.709 (Fig. 5B; 95% CI 57.4 to 84.4%, sensitivity 80.0%, 95% CI 62.7 to 90.5%, specificity 60.0%, 95% CI 42.3 to 75.4%).

DISCUSSION

In this study, we developed a nanoscale flow cytometry–based miRNA-containing EV detection assay and conducted analyses involving a sizable and multi-center α-synucleinopathy cohort encompassing 1203 individuals. Our findings reveal significantly increased plasma miR-44438–containing EV levels in patients with PD, MSA, or iRBD, compared to patients with PSP or HCs. However, there are no significant differences between PD and MSA. Notably, plasma miR-44438–containing EV levels exhibited an inverse correlation with H&Y scales in patients with PD. This result was further supported through the investigation of a longitudinal cohort consisting of 88 patients with PD. Impressively, there was a significant decrease in plasma miR-44438–containing EV levels following an average interval of 16.3 months.

To our knowledge, this study represents an attempt to evaluate miRNA-containing EVs in blood using nanoscale flow cytometry as a diagnostic biomarker for PD and related diseases. In our prior study, we reported increased miR-44438 in neuron-derived EVs from PD patients' blood compared to controls (*8*). miR-44438 contributes to α-syn accumulation by targeting the mRNA of NDST1 and down-regulating the synthesis of heparan sulfate (HS). Several studies have consistently reported that EVs originating from neurons can cross the blood-brain barrier and have been detected in peripheral blood. These findings collectively suggest the potential of miR-44438–containing EV as a biomarker for PD and other α-synucleinopathies.

However, detecting miRNAs in biofluids remained constrained by various limitations. Several miRNA detection methods such as solid-based Northern blotting, microarrays, solution-based polymerase chain reaction, and next-generation sequencing have been extensively reviewed (*17*), highlighting their respective shortcomings. Notably, the limited amount of miRNA within EVs and the associated high costs substantially hinder the feasibility of using RNA sequencing for biomarker detection in large cohorts.

Recent strategies have emerged using nanoscale flow cytometry to quantify targeted EV levels in neurodegenerative diseases (*18*, *19*). Neuron-derived EVs were identified using NMDAR2A and L1CAM (*9*), while CD62P was used as a marker for platelet-derived EVs (*12*). However, nanoscale flow cytometry assays assessing specific miRNA-positive EVs have been lacking because of the absence of robust and specific miRNA probes. The recently developed NCMB probe addresses this limitation by substantially enhancing the fluorescence of MBs, enabling the detection of miRNAs within EVs (*16*).

In this study, the NCMB probe was used to evaluate miR-44438–containing EVs in the plasma of patients diagnosed with PD or related diseases. The marked increase of plasma miR-44438–containing EVs suggests its potential as a diagnostic biomarker for these diseases or conditions. While the levels of miR-44438–containing EVs in patients with PSP are higher than in HCs, they are significantly lower compared to those in patients with PD and patients with MSA. One possible explanation for the increase of miR-44438–containing EVs in patients with PSP could be attributed to the coexistence of both α-syn and tau pathologies. However, this result does not rule out the possibility that miR-44438 can be implicated in non-synuclein pathologies, which should be investigated in the future.

In addition, HS plays a pivotal role in the exocytosis of α-syn in neurons. The up-regulation of miR-44438 within dopaminergic neurons induces α-syn deposition and cellular deficits through the NDST1-HS pathway. This pathway presents a potential mechanism and promising therapeutic target for addressing the pathology of PD and other synucleinopathies.

The inverse correlation of plasma miR-44438–containing EVs with PD patients' H&Y scales and the significant decline over 16.3 months indicate that this biomarker experiences a notable increase at the onset of PD but diminishes as the disease progresses, indicating its potential utility in early or prodromal PD diagnosis. In previous work, we reported that miR-44438 targets NDST1 mRNA, which plays a role in α-syn accumulation in neurons. Excessive α-syn is known to lead to deficits in dopaminergic neurons (*8*). A possible explanation for the observed reduction in miR-44438–positive EV levels in advanced stages of PD could be the depletion of neurons. This hypothesis is supported by the fact that miR-44438 was initially identified in neuron-derived EVs, with over half of these EVs being of neuronal origin, as indicated by L1CAM or NMDAR2A positivity.

Patients with iRBD are considered prodromal for α-synucleinopathies, as they have yet to manifest motor deficits (*20*). Intriguingly, plasma miR-44438–containing EV levels were significantly higher in patients with iRBD versus controls, although only around half of PD/MSA levels. This aligns with the notion of rising miR-44438–containing EV levels before motor symptom onset, in line with the early occurrence of α-syn pathology. However, the value of this biomarker in predicting iRBD phenoconversion remains unexplored and requires longitudinal follow-up studies.

Our findings reveal a decline in miR-44438–containing EV levels as PD progresses, potentially falling into the range seen in healthy individuals at late stages. Notably, early PD diagnosis poses the biggest challenge,

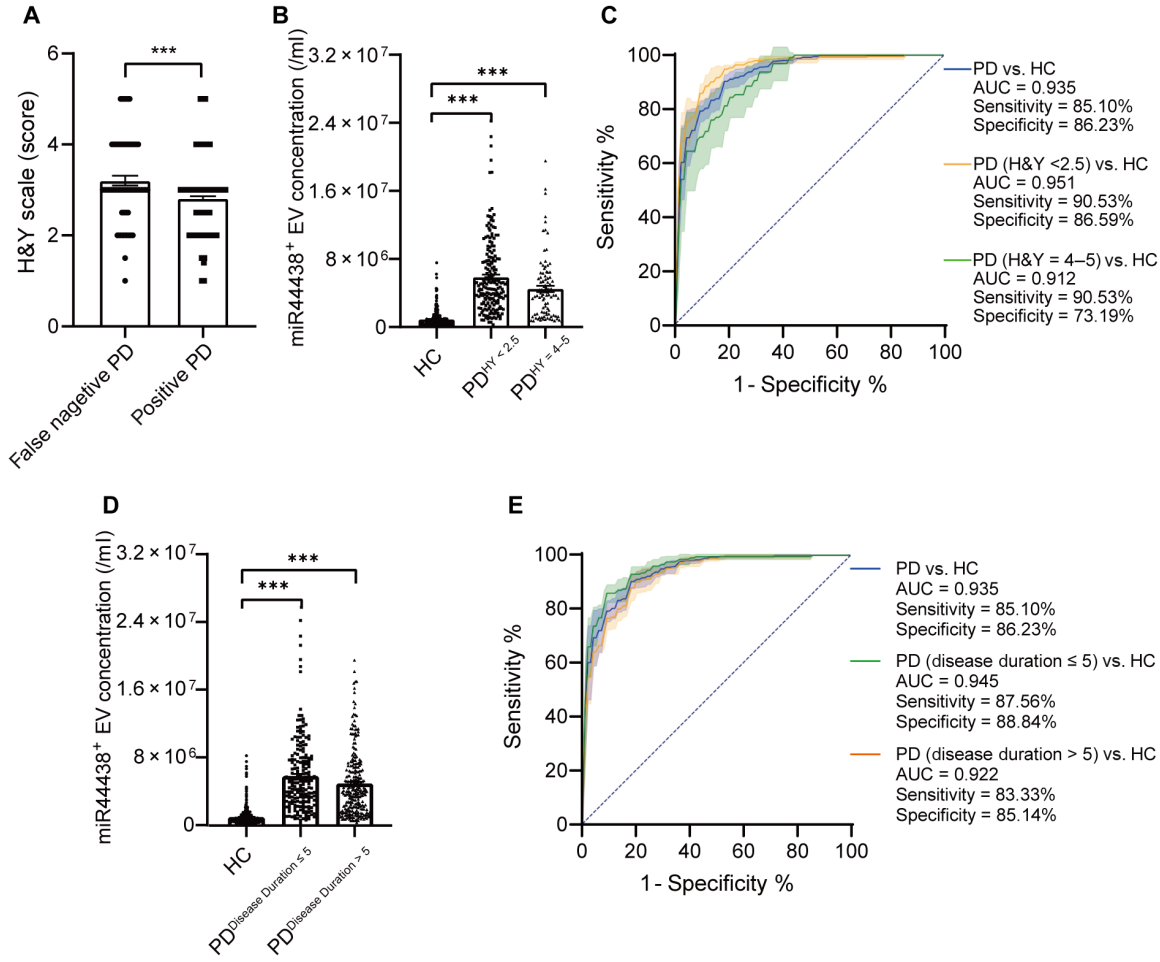

Fig. 4. Diagnostic performance of plasma miR-44438–containing EVs for early-stage PD. (**A**) Comparison of H&Y scales between false-negative and true-positive patients with PD. ***$P < 0.001$. (**B**) Comparisons of miR-44438–containing EV concentrations between HCs and patients with PD at H&Y scale < 2.5 or H&Y scale = 4 to 5. (**C**) ROC curves of plasma miR-44438–containing EVs for discriminating all patients with PD and patients with early-stage PD (H&Y < 2.5) or late-stage PD (H&Y = 4 to 5) from HCs. (**D**) Comparison of miR-44438–containing EV concentrations between patients with PD with disease duration less than or exceeding 5 years. (**E**) ROC curves of plasma miR-44438–containing EVs for discriminating all patients with PD, early-stage PD (disease duration ≤5 years), or late-stage PD (disease duration >5 years) from HCs.

and intriguingly, this biomarker proves even more effective for early PD with remarkable accuracy. It is worth mentioning that we did not observe significant differences between patients with PD and patients with MSA. The similar α-syn pathology in PD and MSA brains suggests that the miR-44438–NDST1-HS pathway disruption may also occur in MSA oligodendrocytes where severe α-syn accumulation takes place.

Our study has several strengths. First, we identified miR-44438–containing EV as a robust biomarker for α-synucleinopathies, supported by its involvement in the α-syn pathology in dopaminergic neurons. This discovery holds promise for potential therapeutic approaches. Second, this study marks the first use of the NCMB-based nanoscale flow cytometry assay to detect specific miRNA-containing EVs in biofluids, offering a previously unidentified source of potential disease biomarkers. Third, the diagnosis utility of miR-44438–containing EV for PD was found and verified through a multi-center cohort encompassing a total of 512 patients with PD and 493 HCs across eight China PD centers. Furthermore, we noticed a declining trend of this biomarker over 16.3 months in patients with PD, indicating its potential as a disease progression indicator.

The limitations of this study should also be acknowledged. First, the nanoscale flow cytometry assay provides a rough estimation of EV sizes in blood, measuring EVs from 110 to 500 nm compared to standard beads. However, it does not offer precise EV size distributions, which is a constraint. Second, the EVs are classified into exosomes, microvesicles, and apoptotic bodies based on their size and biogenesis, and the exosomes, which range in size from 30 to 200 nm, have been studied most extensively. However, this assay has difficulty in detecting exosomes under 110 nm because of light scattering limitations, potentially overlooking alterations in small miR-44438–containing exosomes among groups. Future studies using more sensitive platforms like NanoFCM could provide further insights. Third, this biomarker does not effectively distinguish between PD and MSA, a key diagnostic dilemma in α-synucleinopathies (*21*). As miR-44438 is implicated in α-syn accumulation in both PD and MSA (*8*), dual labeling of miR-44438 and a neuron/oligodendrocyte-specific marker could potentially differentiate between PD and MSA. Furthermore, while we have quantified the levels of miR-44438–containing EVs in a cohort of patients with PSP as a non-synucleinopathy control

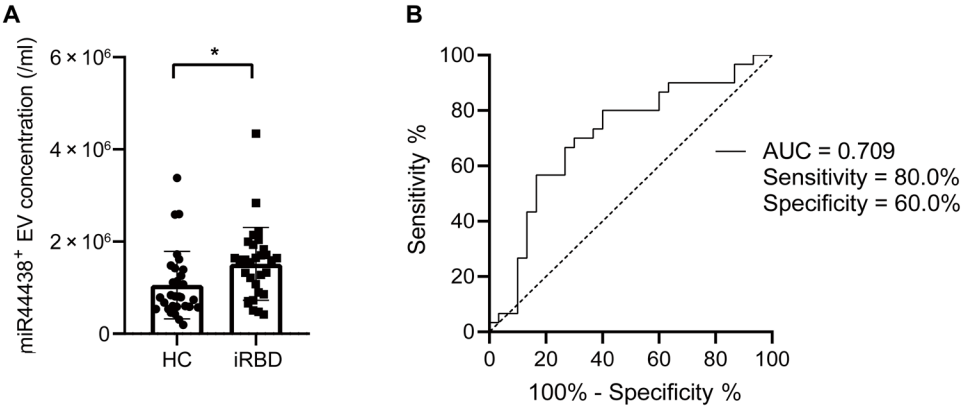

Fig. 5. Levels of plasma miR-44438–containing EVs in patients with iRBD. (**A**) Comparison of plasma miR-44438–containing EV concentrations between patients with iRBD and HCs. *$P < 0.05$. (**B**) ROC curve of plasma miR-44438–containing EV concentrations for discriminating patients with iRBD from HCs.

group, revealing a potential elevation of this biomarker specific to synucleinopathies, it is important to emphasize the necessity of validating this finding in a more extensive cohort including patients with PSP and individuals with other non-synucleinopathy–related conditions in future studies. In addition, all participants in this study were from East Asia. Future research should include cross-racial validation to more conclusively establish the significance and broader applicability of this biomarker.

In summary, this study developed a methodology to quantitatively assess miRNA-containing EVs in blood and provides a robust diagnostic biomarker for PD, MSA, and iRBD with high accuracy. The pronounced efficacy is confirmed through an independent multi-center cohort, underscoring its clinical potential. Our investigation also reveals this biomarker's utility in tracking dynamic disease progression and detecting early disease phases like iRBD. Collectively, this study establishes a promising methodology for probing miRNA-containing EVs in blood and an accurate early detection biomarker for PD and related disorders. Longitudinal studies are needed to elucidate this biomarker's prognostic value in predicting iRBD phenoconversion.

MATERIALS AND METHODS

Participant selection

A total of 1203 participants, including patients with PD, MSA, PSP, and iRBD and HCs, were recruited from Beijing Tiantan Hospital and other seven PD centers in China between March 2019 and April 2023. The diagnosis for patients with PD meets the Movement Disorder Society Clinical Diagnostic Criteria for PD (*22*). All patients with MSA meet the 2008 diagnosis criteria for possible or probable MSA (*23*). Patients with PSP meet the diagnosis criteria for possible or probable PSP (*24*). All participants with iRBD in this study were confirmed through polysomnography and met the International Classification of Sleep Disorders—third edition (ICSD3) diagnostic criteria for iRBD. The exclusion criteria for HC participants include the diagnosis of PD or other neurodegenerative disorders, family history of movement diseases, severe head injury, history of stroke, severe psychiatric disorders, or severe systemic disorders such as schizophrenia, severe depressive or anxiety disorders, and advanced cancers. This study was approved by the ethics committee of Beijing Tiantan Hospital, and written informed consents were obtained from all participants.

For the discovery cohort, we recruited 302 patients with PD, 119 patients with MSA, 21 patients with PSP, and 276 HCs between March 2019 and November 2022 in Beijing Tiantan Hospital. The motor ability of participants was assessed by MDS-UPDRS III and H&Y scale during the OFF medication state. MoCA and MMSE were used for the cognitive function assessment. The Rapid Eye Movement Sleep Behavior Disorder Questionnaire (RBDSQ) was used to assess the disease severity of patients with iRBD. We also recruited a multi-center validation cohort including 208 PD and 217 HCs between November 2022 and April 2023. The inclusion and exclusion criteria were the same as what we used for the discovery cohort. The clinical and demographic characteristics were also recorded. We followed a PD longitudinal cohort of 88 PD participants and remeasured their plasma miR-44438–containing EV levels and clinical characteristics after a mean follow-up time of 16.3 months from the baseline visit.

Postmortem human brain tissues were obtained from the Central Brain & Tissue Bank of Tiantan Hospital and approved by the Ethics Board of the Beijing Tiantan Hospital, Capital Medical University of China (KY 2018-031-02). Informed consents were obtained from all participants or their legal representatives. Midbrain tissues (100 mg each) from a patient with pathology-confirmed PD and three non-PD controls were flash-frozen in liquid nitrogen and subsequently embedded in optimal cutting temperature compound before being sectioned into slices of 5-μm thickness.

miR-44438–NCMB preparation

The preparation of miR-44438–NCMB was conducted following the procedures described previously with slight modifications. Briefly, the NCMB probes were constructed with eight DNA oligonucleotide strands (NCMB1, NCMB2, NCMB3, NCMB4, NCMB-assist, NCMB-anchor, NCMB-BHQ2, and NCMB-cy3) in a specific ratio. All DNA oligonucleotides were resolved in a TAMg buffer [45 mM tris-acetic acid and 12.5 mM magnesium acetate (pH 8.0)] at the concentration of 100 μM. The NCMB1, NCMB2, NCMB3, NCMB4, NCMB-assist, NCMB-anchor, and NCMB-BHQ2 solutions were mixed with the volume ratio of 1:1:1:1:4:1:1 and then annealed (95°C, 5 min; dropped to 80°C, 3 min; dropped to 60°C at a rate of

0.1°C/s; finally dropped to 4°C at a rate of 0.1°C/s) using the C1000 Touch thermal cycler platform (Bio-Rad, USA). Afterward, the NCMB-cy3 oligonucleotide strand was added to the mixture for 1-hour incubation at 37°C to generate the final miR-44438–NCMB. All sequences of the DNA oligonucleotide strands were listed in table S1. The fluorescence of miR-44438–NCMB was assessed using BMG CLARIOStar microplate reader (the excitation and emission wavelength was 550 and 570 nm, respectively; BMG, Germany) with the presence of sequential concentrations of miR-44438 mimic or reference plasma.

TEM analysis

Five microliters of miR-44438–NCMB was applied to a copper grid with a carbon support membrane. After a 60-s incubation, the excess sample was removed with filter paper and stained with a 2% uranyl acetate solution for 60 s. The excess uranyl acetate solution was removed with filter paper and by air-drying. Electron microscope images were collected using a Tecnai F20 TEM at 200 kV.

Nanoscale flow cytometry analysis

Blood samples were drawn from the veins of participants using the BD Vacutainer EDTA blood collection tube (BD Biosciences, CA, USA). The blood was centrifuged at 4°C and 2000*g* for 15 min within 3 hours since collection. The plasma was transferred to a new tube and stored at −80°C for subsequent experiments. Right before the miRNA detection, the plasma was thawed on ice and centrifuged at 4°C and 12,000g for 30 min. Five microliters of plasma from the supernatant was mixed with 50 μl of miR-44438–NCMB at a concentration of 10 nM and incubated at 37°C for 8 hours. After the incubation, we added 150 μl of phosphate-buffered saline (PBS; pH 7.4) to the mixture for a 1:4 dilution and analyzed it using the nanoscale flow cytometry with the Cytoflex S platform (Beckman Coulter, Milano, Italy). To identify small-sized EVs, we used the side scatter mode with a violet excitation laser, which we referred to as violet side scatter (VSSC). Because the VSSC mode introduced a lot of background noise, we used the volumetric measurement to obtain the fluorescence-positive event concentrations (events per milliliter) instead of the ratio of positive to total events. The Apogee Mix (catalog no. 1493) containing 110- and 500-nm green fluorescent polystyrene beads was used for the daily standardization.

Fluorescence staining of brain slices

Midbrain slices were washed with PBS for three times and then blocked using 3% bovine serum albumin in PBS. Following this, the slices were incubated overnight at 4°C with a primary antibody targeting α-syn (1:1000, ab138501, Abcam, UK). Subsequently, they were incubated with a corresponding secondary antibody conjugated with Alexa Fluor 488 for 1 hour at room temperature. The slices were further incubated with miR-44438–NCMB (10 nM) for 8 hours at 37°C, followed by three PBS washes. Nuclei staining was performed using 4′,6-diamidino-2-phenylindole (0.5 μg/ml). Last, the images were captured using a confocal microscope (LSM 710, Carl Zeiss, Germany).

ZetaView NTA analysis

Human plasma samples from 10 HCs, 10 patients with PD, 10 patients with MSA, 10 patients with PSP, and 10 patients with iRBD were centrifuged at 12,000*g* and 4°C for 30 min. Then, 2 μl of plasma supernatant was 1:500 diluted in 0.22-μm filtered PBS. Subsequently, the samples were subjected to the ZetaView (Particle Metrix) platform for nanoparticle distribution and concentration characterization following the manufacturer's instruction.

Statistical analysis

The normality of all data was analyzed using the Kolmogorov–Smirnov test. For the variables not distributing normally, Mann-Whitney *U* and Kruskal-Wallis tests were applied for continuous variables comparison. Binary or multinominal logistic regression was used for group comparisons, incorporating control of covariates such as age, sex, BMI, and LEDD. Bonferroni correction was applied for the analysis of multiple comparisons. A mixed-effects model was used to investigate the temporal changes in miR-44438–containing EV levels, taking into account the variables of sex, age, and BMI. Spearman ranking analysis was used for the associations of plasma biomarkers with clinical characteristics. ROC curve analysis was conducted using Python. Stratified K-fold cross-validation was used to generate the SD values of each AUC plot. *P* value lower than 0.05 was considered statistically significant. All analyses were conducted using GraphPad Prism 8 or Python 3.7.

Supplementary Materials

This PDF file includes:

Figs. S1 to S4
Tables S1 to S3

REFERENCES AND NOTES

1. M. G. Spillantini, M. L. Schmidt, V. M. Lee, J. Q. Trojanowski, R. Jakes, M. Goedert, α-Synuclein in Lewy bodies. *Nature* **388**, 839–840 (1997).
2. A. Schrag, L. Horsfall, K. Walters, A. Noyce, I. Petersen, Prediagnostic presentations of Parkinson's disease in primary care: A case-control study. *Lancet Neurol.* **14**, 57–64 (2015).
3. E. Tolosa, G. Wenning, W. Poewe, The diagnosis of Parkinson's disease. *Lancet Neurol.* **5**, 75–86 (2006).
4. R. B. Postuma, D. Berg, Advances in markers of prodromal Parkinson disease. *Nat. Rev. Neurol.* **12**, 622–634 (2016).
5. K. Burgos, I. Malenica, R. Metpally, A. Courtright, B. Rakela, T. Beach, H. Shill, C. Adler, M. Sabbagh, S. Villa, W. Tembe, D. Craig, K. Van Keuren-Jensen, Profiles of extracellular miRNA in cerebrospinal fluid and serum from patients with Alzheimer's and Parkinson's diseases correlate with disease status and features of pathology. *PLOS ONE* **9**, e94839 (2014).
6. E. Junn, K. W. Lee, B. S. Jeong, T. W. Chan, J. Y. Im, M. M. Mouradian, Repression of α-synuclein expression and toxicity by microRNA-7. *Proc. Natl. Acad. Sci. U.S.A.* **106**, 13052–13057 (2009).
7. J. Kim, K. Inoue, J. Ishii, W. B. Vanti, S. V. Voronov, E. Murchison, G. Hannon, A. Abeliovich, A MicroRNA feedback circuit in midbrain dopamine neurons. *Science* **317**, 1220–1224 (2007).
8. Y. Huang, Z. Liu, N. Li, C. Tian, H. Yang, Y. Huo, Y. Li, J. Zhang, Z. Yu, Parkinson's disease derived exosomes aggravate neuropathology in *SNCA*A53T* mice. *Ann. Neurol.* **92**, 230–245 (2022).
9. C. Tian, T. Stewart, Z. Hong, Z. Guo, P. Aro, D. Soltys, C. Pan, E. R. Peskind, C. P. Zabetian, L. M. Shaw, D. Galasko, J. F. Quinn, M. Shi, J. Zhang; Alzheimer's Disease Neuroimaging Initiative, Blood extracellular vesicles carrying synaptic function- and brain-related proteins as potential biomarkers for Alzheimer's disease. *Alzheimers Dement.* **10**, alz.12723 (2022).
10. Z. Yu, M. Shi, T. Stewart, P. O. Fernagut, Y. Huang, C. Tian, B. Dehay, A. Atik, D. Yang, F. De Giorgi, F. Ichas, M. H. Canron, R. Ceravolo, D. Frosini, H. J. Kim, T. Feng, W. G. Meissner, J. Zhang, Reduced oligodendrocyte exosome secretion in multiple system atrophy involves SNARE dysfunction. *Brain* **143**, 1780–1797 (2020).
11. M. S. Fiandaca, D. Kapogiannis, M. Mapstone, A. Boxer, E. Eitan, J. B. Schwartz, E. L. Abner, R. C. Petersen, H. J. Federoff, B. L. Miller, E. J. Goetzl, Identification of preclinical Alzheimer's disease by a profile of pathogenic proteins in neurally derived blood exosomes: A case-control study. *Alzheimers Dement.* **11**, 600–607 e1 (2015).

12. Z. Wang, Y. Zheng, H. Cai, C. Yang, S. Li, H. Lv, T. Feng, Z. Yu, Aβ1-42-containing platelet-derived extracellular vesicle is associated with cognitive decline in Parkinson's disease. *Front. Aging Neurosci.* **15**, 1170663 (2023).
13. T. Botta-Orfila, X. Morato, Y. Compta, J. J. Lozano, N. Falgas, F. Valldeoriola, C. Pont-Sunyer, D. Vilas, L. Mengual, M. Fernandez, J. L. Molinuevo, A. Antonell, M. J. Marti, R. Fernandez-Santiago, M. Ezquerra, Identification of blood serum micro-RNAs associated with idiopathic and LRRK2 Parkinson's disease. *J. Neurosci. Res.* **92**, 1071–1077 (2014).
14. E. Tolosa, T. Botta-Orfila, X. Morato, C. Calatayud, R. Ferrer-Lorente, M. J. Marti, M. Fernandez, C. Gaig, A. Raya, A. Consiglio, M. Ezquerra, R. Fernandez-Santiago, MicroRNA alterations in iPSC-derived dopaminergic neurons from Parkinson disease patients. *Neurobiol. Aging* **69**, 283–291 (2018).
15. W. Tan, K. Wang, T. J. Drake, Molecular beacons. *Curr. Opin. Chem. Biol.* **8**, 547–553 (2004).
16. D. Mao, M. Zheng, W. Li, Y. Xu, C. Wang, Q. Qian, S. Li, G. Chen, X. Zhu, X. Mi, Cubic DNA nanocage-based three-dimensional molecular beacon for accurate detection of exosomal miRNAs in confined spaces. *Biosens. Bioelectron.* **204**, 114077 (2022).
17. M. de Planell-Saguer, M. C. Rodicio, Analytical aspects of microRNA in diagnostics: A review. *Anal. Chim. Acta* **699**, 134–152 (2011).
18. L. Cheng, R. A. Sharples, B. J. Scicluna, A. F. Hill, Exosomes provide a protective and enriched source of miRNA for biomarker profiling compared to intracellular and cell-free blood. *J. Extracell. Vesicles* **3**, 23743 (2014).
19. M. Shi, C. Liu, T. J. Cook, K. M. Bullock, Y. Zhao, C. Ginghina, Y. Li, P. Aro, R. Dator, C. He, M. J. Hipp, C. P. Zabetian, E. R. Peskind, S. C. Hu, J. F. Quinn, D. R. Galasko, W. A. Banks, J. Zhang, Plasma exosomal α-synuclein is likely CNS-derived and increased in Parkinson's disease. *Acta Neuropathol.* **128**, 639–650 (2014).
20. A. Iranzo, E. Tolosa, E. Gelpi, J. L. Molinuevo, F. Valldeoriola, M. Serradell, R. Sanchez-Valle, I. Vilaseca, F. Lomena, D. Vilas, A. Llado, C. Gaig, J. Santamaria, Neurodegenerative disease status and post-mortem pathology in idiopathic rapid-eye-movement sleep behaviour disorder: An observational cohort study. *Lancet Neurol.* **12**, 443–453 (2013).
21. K. Ubhi, P. Low, E. Masliah, Multiple system atrophy: A clinical and neuropathological perspective. *Trends Neurosci.* **34**, 581–590 (2011).
22. R. B. Postuma, D. Berg, M. Stern, W. Poewe, C. W. Olanow, W. Oertel, J. Obeso, K. Marek, I. Litvan, A. E. Lang, G. Halliday, C. G. Goetz, T. Gasser, B. Dubois, P. Chan, B. R. Bloem, C. H. Adler, G. Deuschl, MDS clinical diagnostic criteria for Parkinson's disease. *Mov. Disord.* **30**, 1591–1601 (2015).
23. S. Gilman, G. K. Wenning, P. A. Low, D. J. Brooks, C. J. Mathias, J. Q. Trojanowski, N. W. Wood, C. Colosimo, A. Durr, C. J. Fowler, H. Kaufmann, T. Klockgether, A. Lees, W. Poewe, N. Quinn, T. Revesz, D. Robertson, P. Sandroni, K. Seppi, M. Vidailhet, Second consensus statement on the diagnosis of multiple system atrophy. *Neurology* **71**, 670–676 (2008).
24. G. U. Hoglinger, G. Respondek, M. Stamelou, C. Kurz, K. A. Josephs, A. E. Lang, B. Mollenhauer, U. Muller, C. Nilsson, J. L. Whitwell, T. Arzberger, E. Englund, E. Gelpi, A. Giese, D. J. Irwin, W. G. Meissner, A. Pantelyat, A. Rajput, J. C. van Swieten, C. Troakes, A. Antonini, K. P. Bhatia, Y. Bordelon, Y. Compta, J. C. Corvol, C. Colosimo, D. W. Dickson, R. Dodel, L. Ferguson, M. Grossman, J. Kassubek, F. Krismer, J. Levin, S. Lorenzl, H. R. Morris, P. Nestor, W. H. Oertel, W. Poewe, G. Rabinovici, J. B. Rowe, G. D. Schellenberg, K. Seppi, T. van Eimeren, G. K. Wenning, A. L. Boxer, L. I. Golbe, I. Litvan; Movement Disorder Society-endorsed PSP Study Group, Clinical diagnosis of progressive supranuclear palsy: The movement disorder society criteria. *Mov. Disord.* **32**, 853–864 (2017).

Acknowledgments

Funding: This research was funded by National Natural Science Foundation of China 82071422 (to T.F.), 82020108012 (to Z.Y.), and 82071417 (to Y.H.) and Beijing Municipal Natural Science Foundation 7212031 (to T.F.) and 7232013 (to Z.Y.). **Author contributions:** Conceptualization: Z.Y., Y.Z., and T.F. Methodology: Z.Y. and Y.Z. Investigation: Z.Y., Y.Z., and T.F. Sampling: H.C., S.L., G.L., W.K., C.Y., S.C., L.C., X. Liu, Z.W., N.Z., X. Li, G.C., Y.C., H.L., and Y.H. Visualization: Z.Y. Supervision: Z.Y. and T.F. Writing—original draft: Z.Y. Writing—review and editing: Y.Z., T.F., H.C., S.L., G.L., W.K., and C.Y. **Competing interests:** The authors declare that they have no competing interests. **Data and materials availability:** All data needed to evaluate the conclusions in the paper are present in the paper and/or the Supplementary Materials.

Submitted 30 October 2023
Accepted 10 April 2024
Published 15 May 2024
10.1126/sciadv.adl6442